

# Photon coincidence spectroscopy for two-atom cavity quantum electrodynamics

L. Horvath and B. C. Sanders

Received: 2000 / Revised version:

## Abstract

We show that photon coincidence spectroscopy can provide an unambiguous signature of two atoms simultaneously interacting with a quantised cavity field mode. We also show that the single-atom Jaynes-Cummings model can be probed effectively via photon coincidence spectroscopy, even with deleterious contributions to the signal from two-atom events. In addition, we have explicitly solved the eigenvectors and eigenvalues of two two-level atoms coupled to a quantised cavity mode for differing coupling strengths.

## 1 Introduction

Photon coincidence spectroscopy (PCS) has been introduced as a tool for probing the spectrum of the Jaynes-Cummings (JC) model corresponding to a single two-level atom (2LA) coupled to one quantised field mode of an optical resonator. Such a system is realised via atomic beam cavity quantum electrodynamics (CQED) [1, 2, 3, 4, 5, 6, 7, 8, 9, 10]. In two-photon coincidence spectroscopy (2PCS), a sparse atomic beam traversing the optical cavity is driven off-axis by a bichromatic driving field, and two photons in the output field of the cavity are deemed to be coincident if they arrive at the photodetectors within some short time interval [6, 9]. During the 2LA's passage through the cavity, the electric dipole coupling strength  $g(\mathbf{r})$  varies with its position  $\mathbf{r}$ , and the coupling strength peaks at an antinode along the cavity's longitudinal axis. The 2LAs are assumed to be sufficiently slowly moving so that the system can be treated as a JC stationary

system with a coupling strength  $g$  varying according to the probability distribution  $P(g)$ . Thus, atomic motion is responsible for an effective inhomogeneous broadening of the spectrum for the coupled atom–cavity system. However, the bichromatic driving field selectively excites a subensemble of coupled atom–cavity systems (with particular values of  $g$ ) to the second couplet of the JC ladder. The JC spectrum is then probed via two–photon coincidence spectroscopy by measuring the rate of two–photon coincidence events, which is referred to as the two–photon coincidence rate (2PCR) [6, 9].

A bichromatic driving field has been used in optical CQED [4], but photon coincidence measurements are yet to be implemented in experiments. More recently experiments have succeeded in controlling, to some extent, single–atom motion in the cavity [11], but complete confinement of a single atom in a cavity [12, 13] with  $P(g) \propto \delta(g - g_0)$ , i.e. a ‘frozen’ atom, is yet to be achieved. 2PCS is designed specifically to overcome inhomogeneous broadening due to atomic motion, thereby permitting the nonlinear component of the JC spectrum (specifically the second couplet of the JC ladder and its two photon de–excitation events) to be optically probed.

2PCS has been shown to be effective for overcoming the challenges of inhomogeneous broadening due to atomic motion. However, a second challenge is atom number fluctuations. As the atoms arrive at the cavity randomly in an atomic beam, the number of atoms in the cavity changes: most of the time no atom is in the cavity; some of the time there is one atom; less frequently there are two or more atoms in the cavity.

In quantum trajectory simulations of 2PCS, multi–atom effects have been included in the simulations [6], and the nonlinear regime of the JC spectrum may be observed even in the presence of multi–atom contributions to the photon statistics. Of course a sparse beam of 2LAs is required to ensure that multi–atom effects do not overwhelm the photon statistics. Rigorous bounds on the mean atom number in CQED have been established [14]. Here we investigate in detail the contributions of multi–atom effects to the extraction of an unambiguous signature of the JC spectrum. We show additional peak structure that arises in the two–photon coincidence spectrum due to the two–2LA contributions, but we also show that these effects can be negligible for a sparse beam. An effect of multi–atom contributions to the 2PCR is to raise the background 2PCR, thereby making 2PCS only marginally more difficult than if two–atom effects could be

avoided altogether.

Furthermore, we consider the system of two 2LAs coupled to a single cavity field mode. For the sparse atomic beam passing through the cavity, we show that an off-axis bichromatic driving field can be used to observe the spectrum of the coupled system consisting of two 2LAs and one quantised cavity field mode. By choosing the two frequencies of the bichromatic driving field judiciously, one may extract the spectrum for various choices of coupling strengths  $g_1$  and  $g_2$  for atoms 1 and 2, respectively. The case  $g_1 = g_2$  corresponds to probing the two-atom version of the Tavis-Cummings model [15].

We develop the Hamiltonian for multi-atom systems in section 2. In section 3, we develop 2PCS as a tool for probing the spectrum of two atoms coupled to a single quantised cavity field mode, and we conclude in section 4.

## 2 Mathematical background

In the typical CQED experiment, which tests for quantum field effects, an atomic beam is directed through a cavity [4, 16] and is excited by a driving field during the passage of the atom. In contrast to microwave cavity quantum electrodynamics [5, 17], where the atomic lifetime is large compared to the passage time through the cavity, the lifetime in an optical system is quite short, hence the need for optically driving the system during the passage of the atom through the cavity. Whereas current experiments employ an on-axis driving field (the laser field is directed into the cavity mode through one mirror), 2PCS is dramatically improved for an off-axis driving field (the atoms are driven directly during passage through the cavity by a bichromatic driving field), and photon coincidences are detected in the cavity output field.

### 2.1 The Hamiltonian

The Hamiltonian for the cavity field is given by

$$H^{(0)} = \hbar\omega a^\dagger a , \quad (1)$$

for  $n = a^\dagger a$  the photon number operator, and  $\omega$  is the angular frequency of the cavity mode (assumed to be equal to the transition

frequency for the 2LA). If there are  $N$  2LAs in the cavity, the Hamiltonian for the  $m^{\text{th}}$  2LA is generalised from  $H^{(0)}$  of equation (1) to yield

$$H^{(m)}(g_m) = \hbar\omega\sigma_z^{(m)} + i\hbar\left(g_m a^\dagger \sigma_-^{(m)} - g_m^* a \sigma_+^{(m)}\right), \quad (2)$$

with  $g_m \equiv g(\mathbf{r}_m)$  the coupling strength between the  $m^{\text{th}}$  atom and the cavity field. Although the atom is moving, we assume that the motion is slow so that time-dependence of the Hamiltonian can be ignored. Atomic motion is then accounted for by allowing  $g_m$  to be a random variable [6, 9]. Taking  $g_m = |g_m| \exp(i\theta_m)$ , and applying a unitary transformation  $U^{(m)}(g_m) = \exp(i\theta_m \sigma_z^{(m)})$  to equation (2), the Hamiltonian simplifies to

$$[U^{(m)}]^\dagger(g_m) H^{(m)}(g_m) U^{(m)}(g_m) = H^{(m)}(|g_m|). \quad (3)$$

Thus, we use the simpler Hamiltonian (3) for treating the  $m^{\text{th}}$  atom and assume that  $g_m$  is real and positive. The 2PCR is a function of the two-photon correlation

$$w^{(2)}(t) = \langle : n(t_0) n(t_0 + t) : \rangle \quad (4)$$

for an unimportant ‘initial’ time  $t_0$ , and ‘:’ imposes normal ordering. The time interval for coincidences is assumed to be short so that the 2PCR is approximately proportional to [6, 7, 9]

$$w^{(2)} = \langle : n^2 : \rangle. \quad (5)$$

The atomic beam is slowly moving, and the time dependence of  $g_m$  can be ignored by instead considering a distribution  $P(g_m)$  for the varying coupling strength of the  $m^{\text{th}}$  2LA. For the multi-atom system, each atom experiences a varying coupling strength. We assume a cut-off of  $N$  atoms in the system; more than  $N$  atoms introduces a negligible effect to measurable quantities. We can express the coupling strength for the  $N$  atoms by the multivariable coupling-strength distribution  $P(\vec{g})$  for  $\vec{g} \equiv (g_1, g_2, \dots, g_N)$ . The Hamiltonian for  $N$  2LAs in the cavity is given by

$$H_N(\vec{g}) = H^{(0)} + \sum_{m=1}^N H^{(m)}(g_m). \quad (6)$$

Under the unitary transformation

$$U_N(\vec{g}) = U^{(N)}(g_N) \otimes U^{(N-1)}(g_{N-1}) \cdots U^{(2)}(g_2) \otimes U^{(1)}(g_1), \quad (7)$$

equation (6) reduces to

$$U_N^\dagger(\vec{g})H_N(\vec{g})U_N(\vec{g}) = \hbar\omega a^\dagger a + \sum_{m=1}^N \hbar\omega\sigma_z^{(m)} + i\hbar g_m \left( a^\dagger \sigma_-^{(m)} - a \sigma_+^{(m)} \right), \quad (8)$$

where we assume that  $g_m$  is always real and positive. The assumption is valid because  $w^{(2)}(t)$  in equation (4) is invariant under unitary transformations by  $U_N(\vec{g})$ .

The case  $H_{M<N}(\vec{g})$ , corresponding to fewer than  $N$  atoms in the cavity, is implicit by setting one or more values of  $g_m$  to be zero. For  $N = 1$  the multiatom Hamiltonian (6) reduces to the JC Hamiltonian [18] with ‘dressed states’

$$|0\rangle \equiv |0\rangle_{\text{cav}} \otimes |\mathbf{g}\rangle \quad (9)$$

and

$$|n\rangle_{\pm} \equiv \frac{i}{\sqrt{2}} (|n-1\rangle_{\text{cav}} \otimes |\mathbf{e}\rangle \pm i|n\rangle_{\text{cav}} \otimes |\mathbf{g}\rangle). \quad (10)$$

Here  $\{|\mathbf{g}\rangle, |\mathbf{e}\rangle\}$  are the ground and excited state of the 2LA. The  $N = 2$  case is developed in detail in Appendix A. Instead of a ladder consisting of a ground state as a singlet and higher-order states as doublets, there is a singlet, then a triplet (for  $n = 1$ ) and then quadruplets (for  $n > 1$ ). This assumes that the two atoms experience different coupling strengths  $g_1 \neq g_2$ . For  $g_1 = g_2$ , the two-2LA Tavis–Cummings model is obtained [15].

## 2.2 The master equation

The Hamiltonian evolution (8) does not account for either irreversible dynamics or contributions from the bichromatic driving field  $\mathcal{E}(t) = \mathcal{E}_1 \exp(-i\omega_1 t) + \mathcal{E}_2 \exp(-i\omega_2 t)$  (with the resonance condition  $\omega_1 = \omega - g_f$ ). To include all these effects, we construct the quantum master equation. The Born–Markov approximation is applied to both radiation reservoirs: the reservoir for the field leaving the cavity and the reservoir for direct fluorescence of the 2LA from the sides of the cavity. The cavity damping rate is  $\kappa$ , and the emission rate into free space is  $\gamma_m$ , where  $\gamma_m$  is the inhibited spontaneous emission rate for the  $m^{\text{th}}$  atom. The master equation [7] can be expressed as  $\dot{\rho} = \mathcal{L}\rho$  for  $\mathcal{L}$  the Liouvillian superoperator and  $\rho$  the density matrix for the system. More specifically the Liouvillian superoperator can be expressed as the sum of a time-independent Liouvillian operator, a time-dependent

Liouvillian operator and a ‘jump’ term. In the rotating frame, the time-independent non-Hermitian effective Hamiltonian is

$$H_{\text{eff}}(\vec{g}) = H_{\text{eff}}^{(0)} + \sum_{m=1}^N H_{\text{eff}}^{(m)}(g_m) \quad (11)$$

with

$$H_{\text{eff}}^{(m)} = \begin{cases} (\omega - \omega_1) a^\dagger a - i\kappa a^\dagger a, & \text{if } m = 0 \\ (\omega - \omega_1) \sigma_z^{(m)} + ig_m(a^\dagger \sigma_-^{(m)} - a \sigma_+^{(m)}) \\ \quad + \Upsilon^{(m)}(\mathcal{E}_1) - i(\gamma_m/2) \sigma_+^{(m)} \sigma_-^{(m)} \end{cases} \quad m > 0. \quad (12)$$

The monochromatic driving term is given by

$$\Upsilon^{(m)}(\mathcal{E}_1) \equiv i\mathcal{E}_1(\sigma_+^{(m)} - \sigma_-^{(m)}). \quad (13)$$

Thus, the Liouville operator for the  $N$ -atom cavity system is

$$\mathcal{L}\rho(\vec{g}) = -\frac{i}{\hbar} \sum_{m=1}^N \left( H_{\text{eff}}^{(m)} \rho(\vec{g}) - \rho(\vec{g}) H_{\text{eff}}^{(m)\dagger} \right) + \mathcal{D}(t; g)\rho + \mathcal{J}\rho \quad (14)$$

with time-dependent driving term

$$\mathcal{D}(t; \delta)\rho = -i \left[ \Upsilon(\mathcal{E}_2 e^{-i\delta t}), \rho(\vec{g}) \right], \quad (15)$$

and jump term

$$\mathcal{J}\rho = 2\kappa a \rho(\vec{g}) a^\dagger + \sum_{m=1}^N \gamma_m \sigma_-^{(m)} \rho(\vec{g}) \sigma_+^{(m)}. \quad (16)$$

We assume that  $\gamma \equiv \gamma_m$  is identical for all atoms. For atom number fluctuations, the 2PCR is the sum of 2PCRs for each case: no atom, one atom, two atoms, and so on. We calculate the 2PCR for each case and add each 2PCR component to obtain the resultant  $w^{(2)}$ , the 2PCR of equation (5), up to an unimportant scaling coefficient. However, the contribution to the 2PCR must be weighted according to the probabilities  $\{p_m\}$ , with  $p_m$  the probability for  $m$  atoms being in the cavity. Thus, the total 2PCR is  $w^{(2)} = \sum_{m=0}^{\infty} p_m w_m^{(2)}$ .

## 2.3 The density matrix

The master equation is used to solve the density matrix  $\rho$  in the long-time limit, well after transients have disappeared. However, the bichromatic driving field results in an oscillatory solution for  $\rho$ ; a time-independent stationary solution is not obtained for this case. The long-time limit for  $\rho$  can be solved by employing a Bloch expansion in terms of the bichromatic driving field frequency difference  $\delta \equiv \omega_2 - \omega_1$ ,

$$\rho(t, \vec{g}) = \sum_{k=0}^{\infty} \rho_k(t, \vec{g}) e^{-ik\delta t}, \quad (17)$$

with  $\rho_k(t, \vec{g})$  time-dependent matrices. In the long-time limit,  $\dot{\rho}_k \approx 0$ , and  $\rho_k(t, \vec{g}) \rightarrow \rho_k(\vec{g})$  is time-independent. As the photocount integration time is expected to be long compared to the frequency  $\delta$ , it is reasonable to approximate  $\rho(t, \vec{g})$  by truncating expansion (17). For photocount integration times larger than  $\delta^{-1}$ , we truncate (17) at  $k = 0$ , yielding  $\rho(t, \vec{g}) \approx \rho_0(\vec{g})$ , which is time-independent. Approximating the time-dependent density matrix by the first (time-independent) term in the Bloch expansion is consistent with single-atom 2PCS studied in reference [7].

The resultant density matrix for the  $N$ -atom cavity system is given by

$$\bar{\rho}(t) \approx \bar{\rho}_0 \equiv \int_{Fg_{\max}}^{g_{\max}} P(\vec{g}) \rho_0(\vec{g}) d\vec{g}, \quad (18)$$

where  $g_{\max}$  is the coupling strength at a cavity antinode,  $Fg_{\max}$  is the effective lower bound cut-off for the coupling ( $0 < F < 1$ ) and  $P(\vec{g}) = P(g_1)P(g_2) \cdots P(g_N)$  is the  $N$ -atom coupling strength distribution, with two typical plots of  $P(g)$  for one atom depicted in figure 1 for  $\kappa$  the cavity loss rate [6, 7]. The effect of averaging over  $P(\vec{g})$  is an inhomogeneous spectral broadening, and we use the overbar  $\bar{\phantom{x}}$  notation to denote averaging over  $P(\vec{g})$  to account for inhomogeneous broadening. This broadening is due to atomic position variability. One distribution (dotted line) corresponds to the case of a uniformly distributed atomic beam entering the cavity and the other (solid line) to an atomic beam initially passing through a rectangular mask [7]. In both cases we have assumed a single-mode cavity supporting a TEM<sub>00</sub> mode and atomic motion perpendicular to the longitudinal axis of the cavity.

### 3 Photon–coincidence spectroscopy for two atoms in the cavity

Although PCS has been developed to probe the nonlinear portion of the (one–atom) JC spectrum (2PCS probes the second couplet and multiphoton coincidence spectroscopy [8] probes higher levels), in this section we show that 2PCS can also probe the nonlinear portion of the spectrum for two–atom events. Interpreting the 2PCR for the two–atom case is somewhat more complicated than for the JC spectrum due to the presence of inhomogeneous broadening for both atoms; methods for interpreting the 2PCR peaks must therefore be more sophisticated. In this section, we describe the method for performing PCS to extract a quantum field signature for two atoms in the cavity.

#### 3.1 Excitation of two atoms coupled to a single cavity mode

Two–atom dressed states are discussed in detail in Appendix A, and this description helps to understand the efficacy of PCS for two–atom CQED. The strong–coupling regime implies that considering atoms and the cavity mode separately is not helpful: dressed states are the preferred description.

The linear portion of the Hamiltonian spectrum consists of the ground state and the one–quantum triplet. This triplet reduces to a doublet for the case that both atoms experience the same coupling strength  $g_1 = g_2$  [15] and is the system being probed in some normal–mode (or vacuum Rabi) splitting experiments which involve multiple atoms in the cavity [1, 2, 3]. Such experiments have been described well by semiclassical theories [19]. The purpose of 2PCS is to extend beyond the linear regime to where quantum field theory is essential for describing observations. Thus, for the two–atom case, 2PCS should be designed to probe the first quadruplet of states (or higher, as an analogy to multiphoton coincidence spectroscopy [8]).

The singlet, triplet and first quadruplet of dressed states for the system consisting of two 2LAs coupled to a single cavity mode are depicted in figure 2(b). Two–photon excitation to the first quadruplet is developed by analogy with two–photon excitation of the JC system to the second doublet, depicted in figure 2(a), and discussed in references [6, 7].



For the (single-atom) JC system in figure 2(a), we depict the two-photon excitation scheme from the ground state  $|0\rangle$  to the first two excited couplets  $|n\rangle_\varepsilon$  ( $n \in \{1, 2\}$ ,  $\varepsilon \in \{-, +\}$ ) of the dressed states. This single-atom system is a useful guide to understanding the two-atom scheme, and we briefly explain the single-atom case here. The challenge is to overcome inhomogeneous broadening of the couplets  $|1\rangle_\varepsilon$  and  $|2\rangle_\varepsilon$  is  $2\hbar g_{\max}$  and  $2\sqrt{2}\hbar g_{\max}$ , respectively, due largely to fluctuations in the atomic position. Two two-photon excitations to the second couplet of the (one-atom) JC system are depicted for a bichromatic driving field with one component of amplitude  $\mathcal{E}_1$  and frequency  $\omega_1$  and the other with amplitude  $\mathcal{E}_2$  and frequency  $\omega_2$ . The excitation pathway on the right of figure 2(a) ( $\omega_1$  then  $\omega_2$ ) excites resonantly from  $|0\rangle$  to  $|1\rangle_-$  and then may excite resonantly from  $|1\rangle_-$  to either of the states  $|2\rangle_\pm$ . The excitation pathway on the left ( $\omega_2$  then  $\omega_1$ ) excites resonantly from  $|0\rangle$  to  $|1\rangle_+$  to  $|2\rangle_-$  for  $g = (\sqrt{2}-1)g_f$ .

For 2PCS, the signature of entanglement is obscured by the background 2PCR due to two  $\omega_2$  photons contributing to excitation to the second couplet via nonnegligible, off-resonant transitions. The method for overcoming this problem is called ‘background subtraction’. In this technique, the experiment is repeated twice, once with the bichromatic driving field and again with the fixed field turned off. The difference between these two 2PCRs shows all the features of the desired 2PCR without the deleterious effects of two  $\omega_2$  transitions to the second couplet states [6, 7].

Now we consider the case of two 2LAs atoms coupled to a single quantised field mode, which is depicted in figure 2(b). Two-photon excitation occurs from the ground state  $|0\rangle$  via the triplet  $|1\rangle_\eta$  to the first quadruplet  $|2\rangle_{\varepsilon\varepsilon'}$  (with  $\eta \in \{-, 0, +\}$  and  $\{\varepsilon, \varepsilon'\} \in \{-, +\}$ ) with  $g_1 \neq g_2$  assumed (the case  $g_1 = g_2$  is sufficiently unlikely to be ignored). Two two-photon excitation pathways to the second couplet are depicted for a bichromatic driving field with one component of amplitude  $\mathcal{E}_1$  and the other with amplitude  $\mathcal{E}_2$ . The excitation pathway on the right ( $\omega_1$  then  $\omega_2$ ) excites resonantly from  $|0\rangle$  to  $|1\rangle_-$  and hence may excite resonantly to any state of the set  $\{|2\rangle_{\varepsilon\varepsilon'}\}$ . The excitation pathway on the left ( $\omega_2$  then  $\omega_1$ ) excites resonantly from  $|0\rangle$  to  $|1\rangle_\eta$  to  $|2\rangle_{\varepsilon\varepsilon'}$ . By analogy with one-atom 2PCR, we can employ a spectral hole-burning approach for excitation to a subensemble of the first quadruplet and thereby operate in the nonlinear regime.

### 3.2 Two-photon coincidence spectrum

For 2PCR of the JC system, the bichromatic driving field is used to excite selectively to subensembles of the inhomogeneous broadened first couplet of the JC ladder, as depicted in figure 2(a). The second photon excites to a state of the second couplet only when the resonance condition for  $\omega_1 + \omega_2$  equals  $2\omega \pm \sqrt{2}g$  for the selected subensemble with coupling strength  $g$ ; this resonance signature provides unambiguous evidence of a quantum field effect through the “ $\sqrt{2}$ ”.

For 2PCR of the two-atom plus cavity mode system, selecting a particular subensemble corresponding to a fixed  $\vec{g} = (g_1, g_2)$  is not possible. To see how this complication arises, consider the case that  $\omega_1$  is tuned such that direct excitation occurs from  $|0\rangle$  to  $|1\rangle_-$ , which is given by equation (22), for certain choices of  $g_1$  and  $g_2$ . The energy of state  $|1\rangle_-$  corresponds to the eigenvalue  $\lambda_-$  of equation (23). Choosing a particular  $\omega_1$  fixes  $\tilde{g} \equiv \sqrt{g_1^2 + g_2^2}$  according to the expression  $\lambda^- = \omega - \tilde{g}$  but does not fix  $g_1$  and  $g_2$  separately. Therefore, choosing a particular  $\omega_1$  does not select a unique subensemble but rather a class of subensembles corresponding to the constraint  $\tilde{g} = \omega - \lambda^- = \omega - \omega_1$ .

This large class of subensembles is not too difficult to manage, however. We are particularly interested in factorisable distributions of the type  $P(\vec{g}) = P(g_1, g_2) = P(g_1)P(g_2)$ ; i.e.  $P(g_m)$  is identical for each independent atom, and  $P(g_i)$  appears as shown in figure 1. Choosing a fixed  $\omega_1$  constrains the selected subensembles to values of  $\tilde{g}$  in the domain of interest, namely large  $\tilde{g}$ , and effectively reduces contributions such as high  $g_1$  and very low  $g_2$  that would negate the desired 2PCR peaks.

For 2PCR of the two-atom-plus-cavity system, the 2PCR is enhanced, not for specific  $g_1$  and  $g_2$  but rather for a range of  $g_1$  and  $g_2$  constrained only by  $\tilde{g}$  being determined by the choice of  $\omega_1$  (and we unfortunately cannot fix both  $g_1$  and  $g_2$  in experimental circumstances). This means that the expected 2PCR peaks are broadened by this limited control of  $g_1$  and  $g_2$ . The 2PCR for two atoms in the cavity, with strong coupling to the mode and a weak bichromatic driving field, is plotted in figure 3.

As an example, we consider the outlying strong peak at  $\tilde{\delta} \doteq 2.414$  (peak *viii* of figure 3(b)). As we will show, this peak is due to the excitation pathway  $|0\rangle \longleftrightarrow |1\rangle_- \longleftrightarrow |2\rangle_{++}$ . The frequency difference for  $|0\rangle \longleftrightarrow |1\rangle_-$  is  $\lambda^-$ , as discussed above, and the transition for  $|1\rangle_- \longleftrightarrow |2\rangle_{++}$  is  $\lambda_1^{++} - \lambda^-$ . The expression for normalised de-

tuning ( $g_f \equiv \omega - \omega_1$ ),

$$\tilde{\delta} = \frac{\omega_2 - \omega}{\omega - \omega_1} = g_f^{-1}(\lambda_1^{++} - \lambda^- - \omega), \quad (19)$$

could be plotted as a line in the three-dimensional space spanned by the  $g_1$ ,  $g_2$  and  $\tilde{\delta}$  axes. We do not present such a plot here but rather note that the trajectory intersects the observed peak value  $\tilde{\delta} \doteq 2.414$  (peak *viii* of figure 3) for  $g_1 = g_{\max}$  and  $g_2 = 0$  or vice versa. This intersection tells us that the peak at  $\tilde{\delta} \doteq 2.414$  is really just a single-atom JC system peak because the second atom is effectively decoupled (negligible  $g_2$ ). Setting the frequency  $\omega_1$  to  $\lambda^\pm$  is therefore not the best way to probe two-atom effects because  $\lambda^\pm$  depends on  $\tilde{g}$  but is not dependent on  $g_1$  and  $g_2$  separately. This has the effect of producing a peak for the case that  $|1\rangle_\pm$  reduces (for  $g_1 = \tilde{g}, g_2 = 0$ ) to  $2^{-1/2}(|0\rangle|\mathbf{e}\rangle \pm |1\rangle|\mathbf{g}\rangle)|\mathbf{g}\rangle$ . Atom 2 remains in the ground state. Similarly, setting  $\omega_1$  to  $\lambda^0$  has the problem that it is completely independent of  $\omega_1$  and  $\omega_2$ .

The dilemma of not having a good choice for  $\omega_1$  to excite from  $|0\rangle$  to  $|1\rangle_\pm$  or  $|1\rangle_0$  is solved by setting  $\omega_2$  to  $\lambda^\pm$  or  $\lambda^0$ . However,  $\omega_2$  is the scanning frequency. The proposal here, though, is first to assume that  $\omega_2$  is set to the frequency  $\lambda^-$ , which excites  $|0\rangle \longleftrightarrow |1\rangle_-$ . Then  $\omega_1 = \lambda^{-+} - \lambda^-$ , which is appropriate for the transition  $|1\rangle_- \longleftrightarrow |2\rangle_{-+}$ . This counter-intuitive choice (letting the scanning frequency excite the first transition rather than the second) enables peak *i* of figure 3 to be understood. The 2PCR would then be enhanced for  $\omega_2 = \lambda^-$  with  $\omega_1$  fixed. The peak corresponding to this excitation pathway (depicted in figure 4) is observed at  $\tilde{\delta} = -1.345$  (peak *i* of figure 3). Substituting this value of  $\tilde{\delta}$  into the expression for  $\tilde{\delta}(g_1, g_2)$  obtained in Appendix A yields the two solutions  $g_1/\kappa = 64.9$  and  $g_2/\kappa = 45.5$  and the reverse. The peak at  $\tilde{\delta} = -1.345$  has its most significant contribution from the case that both atoms contribute to the 2PCR signal.

This analysis helps to understand the 2PCR peak structure depicted in figure 3, but a detailed analysis is afforded by the method of suppressed transitions developed in reference [10]. In this method we identify the specific transitions contributing to each peak.

### 3.3 Method of suppressed transitions

We apply the method of suppressed transitions to understand figure 3 and to identify the peaks corresponding to genuine quantum field ef-

fects for two atoms in the cavity. In the method of suppressed transitions [10], we modify the Liouvillian superoperator  $\mathcal{L}$  in numerical simulations by artificially eliminating particular driving terms responsible for certain peaks. The isolation of specific transitions is obtained by the following procedure. For example, let us consider the influence on the 2PCR of the  $|0\rangle \longleftrightarrow |1\rangle_-$  transition. We can write the effective Hamiltonian (11) for two 2LAs as a matrix in the dressed-state basis. To isolate the influence of the  $|0\rangle \longleftrightarrow |1\rangle_-$  transition, we can set the matrix element  $\langle 0|\Upsilon(\mathcal{E}_1)|1\rangle_-$  and its complex conjugate  $-\langle 1|\Upsilon(\mathcal{E}_1)|0\rangle$  to be zero where  $\Upsilon(\mathcal{E}_1)$  is the (Hermitian) driving term  $\Upsilon(\mathcal{E}_1) = \sum_{m=1}^N \Upsilon^{(m)}(\mathcal{E}_1)$  for  $\Upsilon^{(m)}(\mathcal{E}_1)$  defined by equation (13). In addition the matrix element  $\langle 0|\Upsilon(\mathcal{E}_2 \exp(-i\delta t))|1\rangle_-$  and its complex conjugate can both be set to zero. The jump term  $\mathcal{J}$  is not modified because only the driving terms and their effects are of concern in this analysis of suppressed transitions.

In subsection 3.2, we have shown that transitions from  $|0\rangle$  to  $|1\rangle_\eta$  ( $\eta \in \{-, 0, +\}$ ) via an  $\omega_1$  photon is not the best choice for probing the two-2LA cavity system as these excitations lead to single-atom JC system peaks. The artificial removal of these transitions by the method of suppressed transitions eliminates the (single-atom) JC system peaks in the simulations and thereby helps to identify those peaks that are primarily due to two-atom cavity events. The method of suppressed transitions is a mathematical tool for interpreting peaks in the two-photon spectral structure, not a physical process.

We begin by setting both the matrix element  $\langle 0|\Upsilon(\mathcal{E}_1)|1\rangle_-$  and its complex conjugate to zero as this transition is present in every single-atom peak, and suppressing this transition is an excellent first step to identify peaks associated with two atoms coupled to the cavity mode. The result is depicted in figure 5(a) without and 5(b) with background subtraction. We observe that eliminating these two matrix elements causes a dramatic reduction of peaks *ii*, *iii*, *vi*, *vii*, *viii* with the labelled peak structure of figure 3(b) replicated in figure 5(b) as a dotted line. The reason for these reductions is that the excitation paths responsible for these peaks all have a significant contribution from the  $|0\rangle \longleftrightarrow |1\rangle_-$  transition, employing a photon of frequency  $\omega_1$ . Suppressing  $\langle 0|\Upsilon(\mathcal{E}_1)|1\rangle_-$  and its conjugate only supplies a partial interpretation of the peak structure. A further understanding of these peaks is obtained by imposing the condition that  $-\langle 1|\Upsilon(\mathcal{E}_2 \exp(i\delta t))|2\rangle_{++}$  and its complex conjugate are zero. As shown in figure 6, photon  $\omega_2$  dominates the  $|1\rangle_- \longleftrightarrow |2\rangle_{++}$  tran-

sition responsible for peak *viii*. Thus, the  $\omega_1$ -driven excitation pathway  $|0\rangle \longleftrightarrow |1\rangle_-$  followed by an  $\omega_2$ -driven transition to the  $|2\rangle_{++}$  state is responsible for peak *viii* as shown in figures 5(b) and 6(b), respectively. This method of suppressed transitions validates the analysis of peak *viii* in subsection 3.2, where the excitation pathway  $|0\rangle \longleftrightarrow |1\rangle_- \longleftrightarrow |2\rangle_{++}$  was suggested as being responsible for the existence of this 2PCR peak.

As another example, we consider the transition  $|1\rangle_- \longleftrightarrow |2\rangle_{+-}$ . By eliminating this transition, peak *vii* (and vicinity) are reduced as shown in figure 6(d). Thus, the  $|0\rangle \longleftrightarrow |1\rangle_- \longleftrightarrow |2\rangle_{+-}$  pathway, induced by an  $\omega_1$  photon followed by an  $\omega_2$  photon, is partially responsible for the increase of the 2PCR at *vii* (and vicinity). Figures 5 and 6(f) show clearly that an  $\omega_1$ -driven  $|0\rangle \longleftrightarrow |1\rangle_-$  transition and an  $\omega_2$ -driven  $|1\rangle_- \longleftrightarrow |2\rangle_{--}$  transition are responsible for the background of peaks *iv*, *v* and *vi* but not for the actual peaks themselves. Setting  $-\langle 1|\Upsilon(\mathcal{E}_2 \exp(i\delta t))|2\rangle_{-+}$  and its complex conjugate to zero eliminates peaks *ii* and *iii* as shown in figures 6(g, h). Clearly, peaks *ii* and *iii* are primarily due to a resonant  $|0\rangle \longleftrightarrow |1\rangle_-$  transition via an  $\omega_1$  photon, followed by an excitation via an  $\omega_2$  photon to  $|2\rangle_{-+}$  state. Peaks *ii* and *iii* are the dominant peaks because, apart from the fixed field with frequency  $\omega_1$  driving  $|0\rangle \longleftrightarrow |1\rangle_-$ , the scanning field also drives  $|0\rangle \longleftrightarrow |1\rangle_-$  via an off-resonance transition; thus, higher populations of the  $|2\rangle_{-+}$  is expected.

Thus far, we have identified those peaks that are due to single-atom events. The remaining peaks, particularly *iv*, *v* and *vii*, are the ones of interest because they are primarily due to the two-atom cavity signature, and this is because the transition  $|0\rangle \longleftrightarrow |1\rangle_\eta$  state is via an  $\omega_2$  photon. To explain peaks *iv*, *v* and *vii*, we set  $\langle 0|\Upsilon(\mathcal{E}_2 \exp(-i\delta t))|1\rangle_\eta$  and  ${}_\eta\langle 1|\Upsilon(\mathcal{E}_1)|2\rangle_{\varepsilon\varepsilon'}$ , and their complex conjugates, all to zero. For example, setting  $\langle 0|\Upsilon(\mathcal{E}_2 \exp(-i\delta t))|1\rangle_+$  and its complex conjugate to zero eliminates the peaks at *v*, *vi* and *vii* as shown in figure 7(b). With this result and figure 9(b), we observe that the peak at *vii* is due to an  $\omega_2$ -driven  $|0\rangle \longleftrightarrow |1\rangle_+$  transition followed by an  $\omega_1$ -driven  $|1\rangle_+ \longleftrightarrow |2\rangle_{+-}$  transition. Fixing  ${}_+\langle 1|\Upsilon(\mathcal{E}_1)|2\rangle_{--}$  and its complex conjugate to zero reduces the peak at *vi* as shown in figure 9(d). Thus, the small bump, namely peak *vi* (to the right of peak *v*), is due to an  $\omega_2$ -driven excitation  $|0\rangle \longleftrightarrow |1\rangle_+$  followed by an  $\omega_1$ -driven  $|1\rangle_+ \longleftrightarrow |2\rangle_{--}$  transition. As shown in figure 7(b) and figure 9(f), the removal of the  $\omega_2$ -driven transition  $|0\rangle \longleftrightarrow |1\rangle_+$  and the  $\omega_1$ -driven  $|1\rangle_+ \longleftrightarrow |2\rangle_{-+}$  transition yields a diminished peak

*v*. Peak *iv* is diminished if the transitions  $\langle 0|\Upsilon(\mathcal{E}_2 \exp(-i\delta t))|1\rangle_0$ ,  ${}_0\langle 1|\Upsilon(\mathcal{E}_2 \exp(-i\delta t))|2\rangle_{--}$  and  ${}_0\langle 1|\Upsilon(\mathcal{E}_2 \exp(-i\delta t))|2\rangle_{-+}$ , together with their complex conjugates, are suppressed by being set to zero as shown in figures 7(d), 8(b) and 8(d). Clearly, peak *iv* is due to an  $\omega_2$ -driven resonant pathway  $|0\rangle \longleftrightarrow |1\rangle_0$ , followed by  $\omega_1$ -driven transitions  $|1\rangle_0 \longleftrightarrow |2\rangle_{-+}$  and  $|1\rangle_0 \longleftrightarrow |2\rangle_{--}$ . Finally, peak *i* vanishes if we eliminate the  $\omega_2$ -driven resonant pathway  $|0\rangle \longleftrightarrow |1\rangle_-$  followed by the  $\omega_1$ -driven  $|1\rangle_- \longleftrightarrow |2\rangle_{-+}$  transition (figures 7(e, f) and 8(e, f)).

The clearest unambiguous spectroscopic feature of the two 2LA-cavity system, which cannot be accounted for by the (single-atom) JC-spectrum, is peak *i*. This peak is almost visible in figure 3(a) and clearly visible after background subtraction as shown in figure 3(b). In addition, the peak is much more pronounced than the other relevant 2PCR peaks at *iv*, *v* and *vii*. Thus, this peak provides an ideal signature of quantum field effects in two-atom cavity systems.

Furthermore, the method of suppressed transitions allows us to identify the deleterious two-photon pathways that destroy the quantum signature of single-atom and two-atom peaks (single-atom peaks *ii* and *iii* and two-atom peaks *i*, *iv*, *v* and *vii*). These pathways are responsible for the difference between figure 3(a) and 3(b). Background subtraction eliminates precisely those deleterious pathways. Figures 6(g) and 7(e) clearly show that peaks *i*, *ii* and *iii* are strongly affected by the  $|0\rangle \longleftrightarrow |1\rangle_- \longleftrightarrow |2\rangle_{-+}$  pathway via two  $\omega_2$  photons. The second major undesired pathway washes peaks *iv*, *v*, *vi* and *vii* away. This pathway is primarily due to the  $\omega_2$ -driven transition  $|0\rangle \longleftrightarrow |1\rangle_+$  (as shown in figure 7(a)), followed by an  $\omega_2$ -driven transition  $|1\rangle_+ \longleftrightarrow |2\rangle_{++}$  (not shown).

## 4 Conclusion

For an atomic beam the number of atoms in the cavity mode is a randomly varying quantity. For a sparse beam, most of the time there is effectively no atom in the cavity. A large portion of time there is effectively one atom, although, of course, its position is a randomly varying quantity. There is also a contribution to the photon coincidence spectrum due to two or more atoms simultaneous interacting with the cavity mode. In section 3, we have assumed precisely two atoms in the cavity but left the positions random. In this section we include the signal for one and no atom events in the cavity with

appropriate weightings for a sparse beam. We show that the 2PCR reveals genuine quantum field effects for two-atom events.

We let  $\bar{\rho}_n$  represent the density matrix for  $n$  atoms in the cavity, averaged over the atomic positions. This matrix  $\bar{\rho}_n$  is a generalisation of equation (18) where the subscript refers to the number of atoms in the cavity. For the sparse atomic beam, we will ignore  $\bar{\rho}_n$  for  $n > 2$ . The case  $n = 0$  is not significant because off-axis driving ensures that photon coincidences do not arise when there is no atom present. Here we make the reasonable assumption that  $p_1/p_2 = 9$ . That is, the probability of having one atom in the cavity is nine times more likely than having two atoms. This is compatible with the sparse beam assumption. The result for  $p_1/p_2 = 9$  is shown in figure 10(a, b).

We consider two cases: a high value of  $g_f (= 63\kappa)$  as discussed in subsection 3.3 ( $g_f = 63\kappa$  was assumed in a study of multiphoton coincidence spectroscopy for the JC model [8]), and a low value of  $g_f (= 9\kappa)$ , which has been the subject of other studies of photon coincidence spectroscopy [6, 7, 9]. The case of a high value of  $g_f$  corresponds to strong coupling and is depicted in figure 10(a); the low value case is depicted in figure 10(b).

For  $g_f = 63\kappa$ , we observe that peak  $i$ , which corresponds to a genuine quantum field effect with two strongly coupled atoms in the cavity, is still quite pronounced, despite the strong signal from single-atom effects. Even for  $p_1/p_2 = 9$ , the two-atom events contribute a strong difference-2PCR signal. Therefore, we can assert that two-photon coincidence spectroscopy is an effective means for extracting the quantum field signature of two atoms in a quantised field cavity for a sparse atom beam.

On the other hand, we explore the case of relatively low coupling, namely  $g_f = 9\kappa$ . This case is depicted in figure 10(b) and shows that the single-atom 2PCR spectrum (depicted as a dotted line) is not modified in any substantial way by the two-atom contributions. Therefore, the employment of 2PCS as a probe of quantum field effects in the (single-atom) JC model is sound for a sparse atomic beam. Of course it was assumed in references [6, 7] that multi-atom effects were not significant factors in modifying the ideal single-atom two-photon spectrum. However, here figure 10(b) reveals quite clearly how much of an effect arises from two-atom events and how small this effect is.

On the one hand, for strong coupling, the two-atom effect is large, and peak  $i$ , in particular, can be used to probe experimentally the quantum field effect for two-atom cavity quantum electrodynamics.

On the other hand, for lower coupling strengths, we can safely ignore the effects of rare two-atom events in cavity quantum electrodynamics. The theory presented here allows us to distinguish the two cases and know when two-atom effects are important.

## Acknowledgements

We have benefitted from valuable discussions with H. J. Carmichael. This research has been supported by Australian Research Council Large and Small Grants, by an Australian Research Council International Research Exchange (IREX) grant, by a Macquarie University Research Grant and by the Macquarie University Postgraduate Research Fund.

## A Eigenvectors and eigenvalues for two two-level atoms in a single-mode cavity

The Hamiltonian for two 2LAs in an optical cavity can be derived from equation (8) and is given by

$$\begin{aligned} H = & \hbar\omega a^\dagger a + \hbar\omega\sigma_z^{(1)} + \hbar\omega\sigma_z^{(2)} + i\hbar g_1 \left( a^\dagger \sigma_-^{(1)} - a \sigma_+^{(1)} \right) \\ & + i\hbar g_2 \left( a^\dagger \sigma_-^{(2)} - a \sigma_+^{(2)} \right). \end{aligned} \quad (20)$$

For the one-atom case, the Hamiltonian is diagonalised to yield the JC dressed states. Diagonalising equation (20) for  $g_1 = g_2$  yields the dressed states of the two-2LA Tavis-Cummings system [15]. In this section, we consider the dressed states for  $g_1 \neq g_2$ .

The (one-atom) JC spectrum of figure 2(a) is a ladder of states consisting of a ground state and then a sequence of couplets. The dressed states are designated as  $|n\rangle_\varepsilon$ , with  $n$  designating the couplet number and  $\varepsilon \in \{+, -\}$  designating whether the state is the one with higher or lower energy. The quantity  $n$  corresponds to the number of quanta in the system; for example the states  $|1\rangle_\pm$  are superpositions of  $|1\rangle|g\rangle$  and  $|0\rangle|e\rangle$ , i.e. a superposition of a photon (and the atom in the ground state) with an atomic excitation (and the cavity mode in the ground state). Here we generalise this approach to the case of two 2LAs in the cavity.



The first few levels of the spectral ladder are shown in figure 2(b). The ground state is designated as  $|0\rangle$  and corresponds to an absence of photons in the cavity and both atoms in the ground state. For  $\tilde{g}^2 \equiv g_1^2 + g_2^2$ , the set of one-quantum states form a triplet, and the three eigenstates of this triplet are

$$|1\rangle_0 = \tilde{g}^{-1}|0\rangle(g_2|\mathbf{e}\rangle|\mathbf{g}\rangle - g_1|\mathbf{g}\rangle|\mathbf{e}\rangle) \quad (21)$$

$$|1\rangle_{\pm} = \mp 2^{-1/2}i|0\rangle|\mathbf{g}\rangle|\mathbf{g}\rangle + 2^{-1/2}\tilde{g}^{-1}|0\rangle(g_2|\mathbf{g}\rangle|\mathbf{e}\rangle + g_1|\mathbf{e}\rangle|\mathbf{g}\rangle), \quad (22)$$

with corresponding eigenvalues

$$\lambda^{\pm} = \omega \pm \tilde{g} \quad (\text{for } |1\rangle_{\pm}) \quad (23)$$

$$\lambda^0 = \omega \quad (\text{for } |1\rangle_0), \quad (24)$$

respectively.

The multi-quanta states, for two and more energy quanta, are quadruplets. We use the notion  $|n\rangle_{\varepsilon\varepsilon'}$ , with  $n$  the number of quanta ( $n = 2$  for the first quadruplet,  $n = 3$  for the second, etc.). The subscripts  $\varepsilon$  and  $\varepsilon'$  are each either  $+$  or  $-$  (i.e.  $\varepsilon, \varepsilon' \in \{+, -\}$ ), and there are four distinct combinations of  $\varepsilon\varepsilon'$  corresponding to each of the four states in the quadruplet. The choices of  $\varepsilon$  and  $\varepsilon'$  are determined by signs in the expression for the eigenvalue of the particular state. The four states of the  $n^{\text{th}}$  quadruplet are

$$\begin{aligned} |n+1\rangle_{+\pm} &= \Lambda_{\pm}^{(n)}|n+1\rangle|\mathbf{g}\rangle|\mathbf{g}\rangle - i\zeta_{1\pm}^{(n)}|n\rangle|\mathbf{g}\rangle|\mathbf{e}\rangle \\ &\quad - i\zeta_{2\pm}^{(n)}|n\rangle|\mathbf{e}\rangle|\mathbf{g}\rangle + (\mathcal{N}_{\pm}^{(n)})^{-\frac{1}{2}}|n-1\rangle|\mathbf{g}\rangle|\mathbf{g}\rangle \\ |n+1\rangle_{-\pm} &= \Lambda_{\pm}^{(n)}|n+1\rangle|\mathbf{g}\rangle|\mathbf{g}\rangle + i\zeta_{1\pm}^{(n)}|n\rangle|\mathbf{g}\rangle|\mathbf{e}\rangle \\ &\quad + i\zeta_{2\pm}^{(n)}|n\rangle|\mathbf{e}\rangle|\mathbf{g}\rangle + (\mathcal{N}_{\pm}^{(n)})^{-\frac{1}{2}}|n-1\rangle|\mathbf{g}\rangle|\mathbf{g}\rangle. \end{aligned}$$

The coefficients employ the convenient terms

$$\begin{aligned} \Xi^{(n)} &= \sqrt{(2n+1)^2(g_1^2 + g_2^2)^2 - 4n(n+1)(g_1^2 - g_2^2)^2}, \\ \Lambda_{\pm}^{(n)'} &= -\frac{(g_1^2 + g_2^2 \pm \Xi^{(n)})}{4g_1g_2\sqrt{n(n+1)}}, \\ \zeta_{1\pm}^{(n)'} &= \frac{g_2^2 + g_1^2(1+4n) \pm \Xi^{(n)}}{2g_2\sqrt{2n((2n+1)(g_1^2 + g_2^2) \pm \Xi^{(n)})}}, \\ \zeta_{2\pm}^{(n)'} &= \frac{g_1^2 + g_2^2(1+4n) \pm \Xi^{(n)}}{2g_1\sqrt{2n((2n+1)(g_1^2 + g_2^2) \pm \Xi^{(n)})}}, \end{aligned}$$

with

$$\mathcal{N}_{\pm}^{(n)} = \Lambda_{\pm}^{(n)'}{}^2 + \zeta_{1\pm}^{(n)'}{}^2 + \zeta_{2\pm}^{(n)'}{}^2 + 1,$$

$$\Lambda_{\pm}^{(n)} = \frac{\Lambda_{\pm}^{(n)'}}{\sqrt{\mathcal{N}_{\pm}^{(n)}}}, \quad \zeta_{1\pm}^{(n)} = \frac{\zeta_{1\pm}^{(n)'}}{\sqrt{\mathcal{N}_{\pm}^{(n)}}}, \quad \zeta_{2\pm}^{(n)} = \frac{\zeta_{2\pm}^{(n)'}}{\sqrt{\mathcal{N}_{\pm}^{(n)}}}.$$

The corresponding eigenvalues of the  $n$  quadruplet are

$$\lambda_n^{\pm\pm} = (n+1)\omega \pm \sqrt{\frac{(2n+1)(g_1^2 + g_2^2) \pm \Xi^{(n)}}{2}} \text{ (for } |n+1\rangle_{\pm\pm}\text{)}, \quad (25)$$

$$\lambda_n^{\mp\pm} = (n+1)\omega \mp \sqrt{\frac{(2n+1)(g_1^2 + g_2^2) \pm \Xi^{(n)}}{2}} \text{ (for } |n+1\rangle_{\mp\pm}\text{)}. \quad (26)$$

For this analysis, we have assumed that  $g_1 \neq g_2$ . If  $g_1 = g_2$ , we obtain the Tavis–Cummings model [15], for which the ladder consists of a ground state singlet, a doublet for the one–quantum states (with an energy splitting  $\sqrt{2}g$ ) and then triplets for two or more quantum states. As this case has been studied in depth, we do not analyse the Tavis–Cummings model here.

## References

- [1] RAIZEN, M. G., THOMPSON, R. J., BRECHA, R. J., KIMBLE, H. J., and CARMICHAEL, H. J., 1989, *Phys. Rev. Lett.*, **63**, 240–243.
- [2] ZHU Y., GAUTHIER, D. J., MORIN S. E., WU, Q., CARMICHAEL, H. J., and MOSSBERG, T. W., 1990, *Phys. Rev. Lett.*, **64**, 2499–2502.
- [3] THOMPSON, R. J., REMPE, G., and KIMBLE, H. J., 1992, *Phys. Rev. Lett.*, **68**, 1132–1135.
- [4] TURCHETTE Q. A., HOOD C. J., LANGE, W., MABUCHI, H., and KIMBLE, H. J., 1995, *Phys. Rev. Lett.*, **75**, 4710–4713.
- [5] BRUNE, M., SCHMIDT–KALER, F., MAALI, A., DREYER, J., HAGLEY, E., RAIMOND, J. M., and HAROCHE, S., 1996, *Phys. Rev. Lett.*, **76**, 1800–1803.
- [6] CARMICHAEL, H. J., KOCHAN P., and SANDERS, B. C., 1996, *Phys. Rev. Lett.*, **77**, 631–634.
- [7] SANDERS, B. C., CARMICHAEL, H. J., and WIELINGA, B. F., 1997, *Phys. Rev. A*, **55**, 1358–1370.

- [8] HORVATH, L., SANDERS, B. C., and WIELINGA, B. F., 1999, *J. Opt. B: Quant. and Semiclassical Opt.*, **1**(4), 446–451.
- [9] HORVATH, L., and SANDERS, B. C., 2000, *Phys. Rev. A* (in press); quant-ph/0011079.
- [10] HORVATH, L., and SANDERS, B. C., 2001, *Aust. J. Phys.* (accepted), quant-ph/0012002.
- [11] HOOD, C. J., LYNN, T. W., DOHERTY, A. C., PARKINS, A. S., and KIMBLE, H. J., 2000, *Science* **287**, 1447; PINKSE, P. W. H., FISCHER, T., MAUNZ, P., and REMPE, G., 2000, *Nature*, **404**, 365.
- [12] DOHERTY, A. C., LYNN, T. W., HOOD, J. C., and KIMBLE, H. J., 2001, *Phys. Rev. A*, **63**, 013401.
- [13] PARKINS, A. S., and KIMBLE, H. J., 2000, *Phys. Rev. A*, **61**, 052104.
- [14] CARMICHAEL, H. J., and SANDERS, B. C., 1999, *Phys. Rev. A*, **60**, 2497–2504.
- [15] TAVIS, M., and CUMMINGS, F. W., 1968, *Phys. Rev.*, **170**(2), 379; TAVIS, M., and CUMMINGS, F. W., 1969, *Phys. Rev.*, **188**(2), 692.
- [16] FOSTER, G. T., OROZCO, L. A., CASTRO-BELTRAN, H. M., and CARMICHAEL, H. J., 2000, *Phys. Rev. Lett.*, **85**, 3149–3152.
- [17] SCULLY, M. O., MEYER, G. M., and WALTHER, H., 1996, *Phys. Rev. Lett.*, **76**, 4144–4147.
- [18] JAYNES, E. T., and CUMMINGS, F. W., 1963, *Proc. IEEE*, **51**, 89–109.
- [19] CARMICHAEL, H. J., TIAN, L., and REN, W., 1994, Nonperturbative atom–photon interactions in an optical cavity. In *Cavity quantum electrodynamics*, edited by P. R. BERMAN (Boston: Academic Press), pp. 381–423.

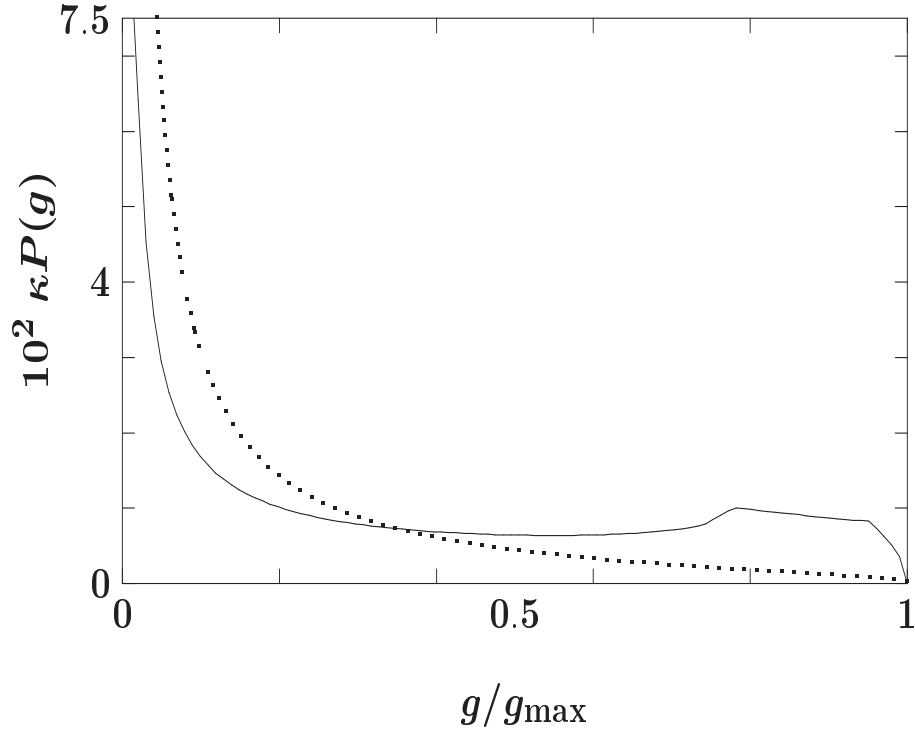


Figure 1: The scaled coupling strength distributions  $\kappa P(g)$  as a function of  $g/g_{\max}$  for single atoms passing through an optical cavity supporting a single  $\text{TEM}_{00}$  mode. The solid curve corresponds to a typical distribution for a rectangular mask filtering the atomic beam. The dotted line corresponds to the absence of a mask.

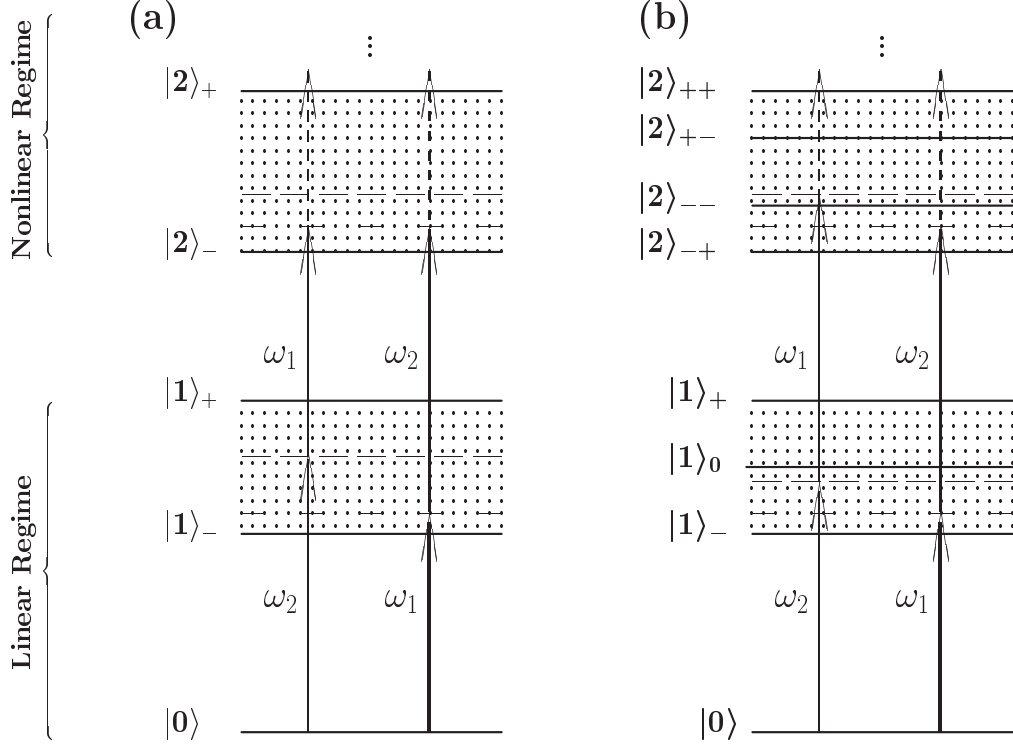


Figure 2: The lowest dressed-state multiplet in the nonlinear regime for (a) the Jaynes-Cummings system and (b) two two-level atoms coupled to a single quantised field mode of the cavity. Each system may be driven by a bichromatic field with frequencies  $\omega_1$  and  $\omega_2$ . Two excitation pathways to the second multiplet are depicted in each case. Inhomogeneous broadening of multiplets is depicted by the shaded region. In case (a), the first doublet has inhomogeneous broadening  $2g_{\max}$ , and the second has width  $2\sqrt{2}g_{\max}$ . In case (b), the triplet has an inhomogeneous broadening width of  $2\sqrt{2}g_{\max}$ .

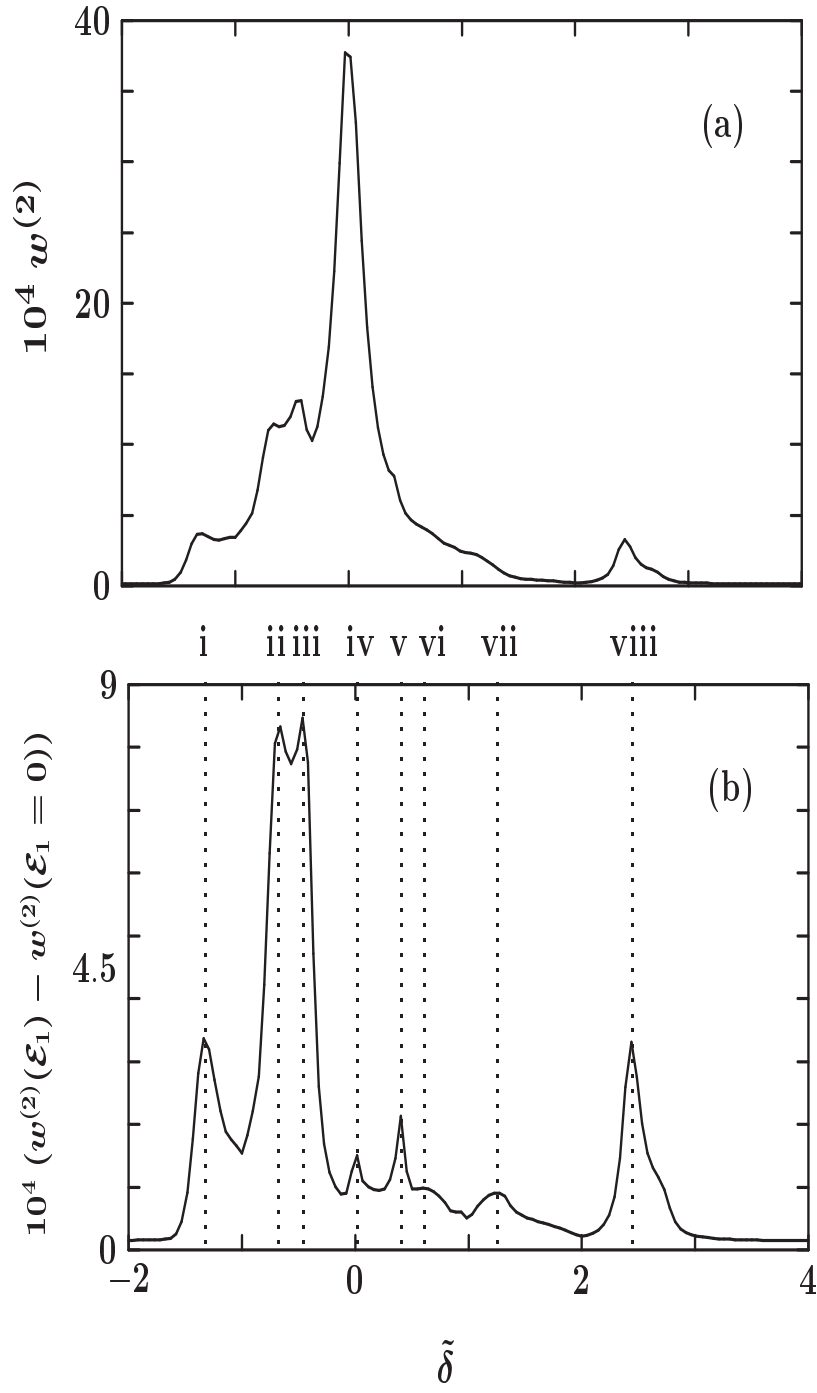


Figure 3: Two-photon count rate vs normalised scanning frequency for two atoms in a sparse atomic beam for  $\tilde{g} = g_f = 63\kappa$ ,  $\mathcal{E}_1/\kappa = 1/\sqrt{2}$ ,  $\mathcal{E}_2/\kappa = \sqrt{2}$  and  $\gamma/\kappa = 2$  (a) without and (b) with background subtraction. Vertical dotted lines are placed in (b) to identify the obvious peaks.

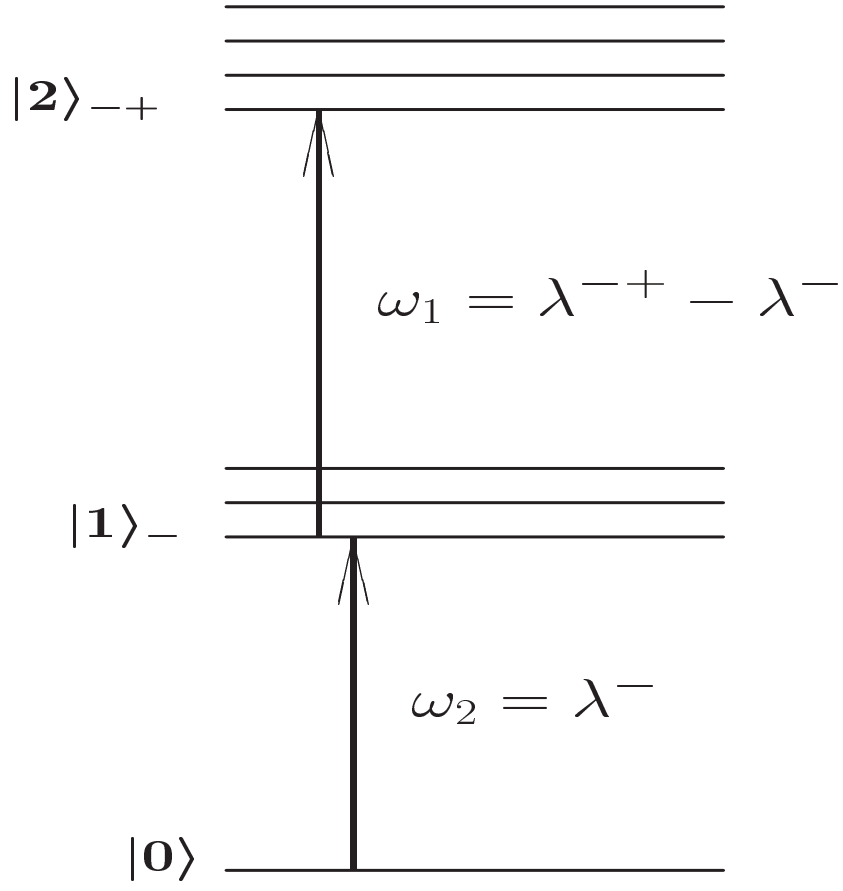


Figure 4: The excitation pathway responsible for the two-atom signature in 2PCS.

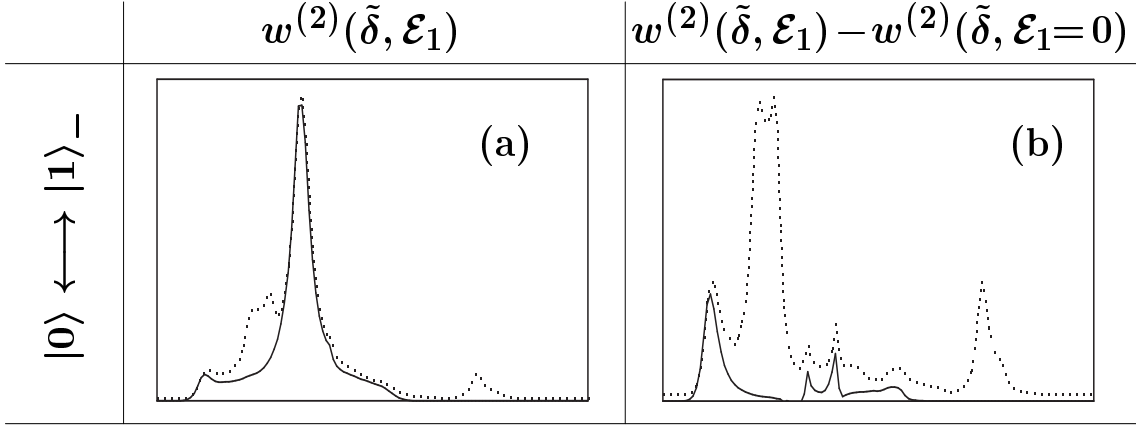


Figure 5: The 2PCR (a) without and (b) with background subtraction as a dotted line. The solid line is the 2PCR for the  $\omega_1$ -driven  $|0\rangle \longleftrightarrow |1\rangle_-$  transition artificially suppressed in the simulations. The dotted lines are replicates of those in figure 3(a, b), and the scales here correspond to those scales.



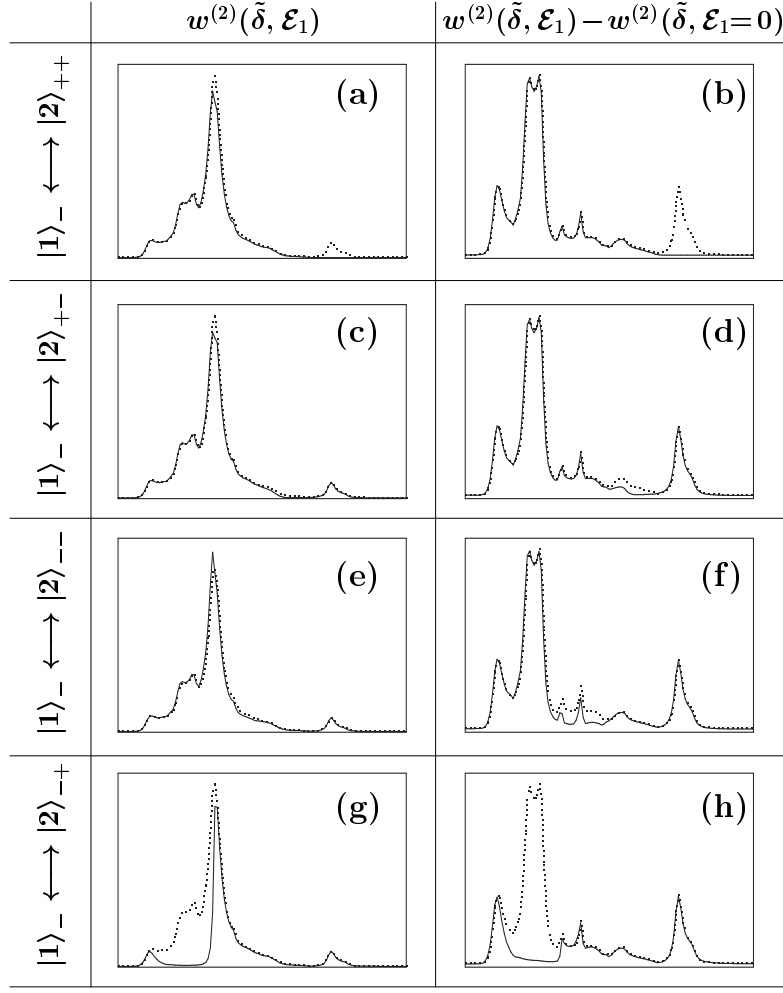


Figure 6: The 2PCR without (first column) and with (second column) background subtraction as the dotted line. The solid line corresponds to the 2PCR for an  $\omega_2$ -driven transition artificially suppressed in the numerical simulation. The suppressed transition is  $|1\rangle_- \longleftrightarrow |2\rangle_{++}$  for the first row,  $|1\rangle_- \longleftrightarrow |2\rangle_{+-}$  for the second row,  $|1\rangle_- \longleftrightarrow |2\rangle_{--}$  for the third row and  $|1\rangle_- \longleftrightarrow |2\rangle_{-+}$  for the fourth row.

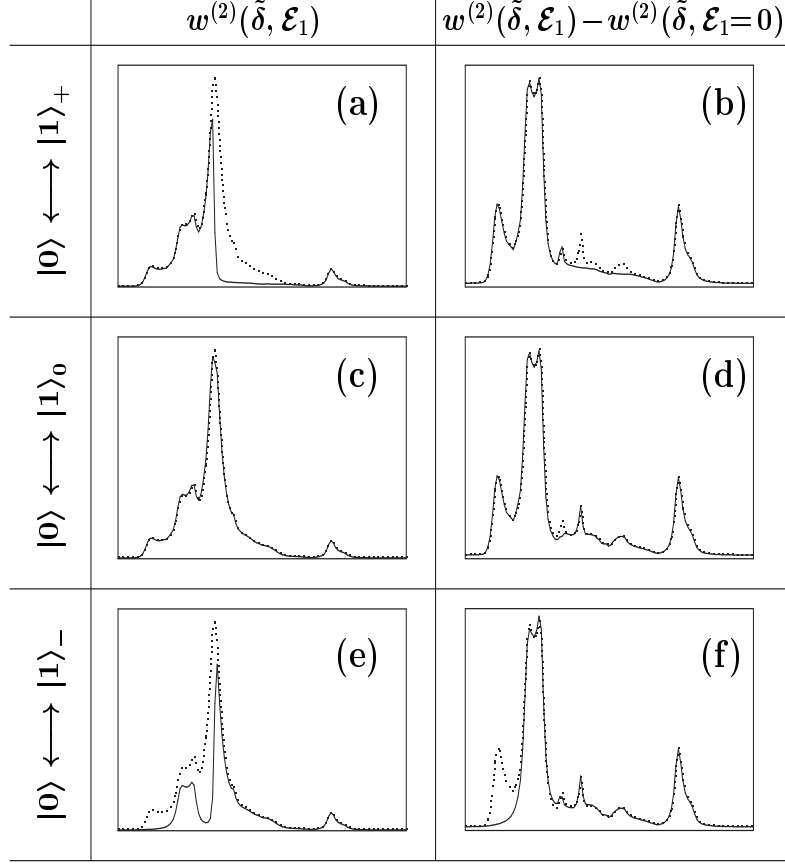


Figure 7: The 2PCR without (first column) and with (second column) background subtraction as the dotted line. The solid line corresponds to the 2PCR for an  $\omega_2$ -driven transition artificially suppressed in the numerical simulation. The suppressed transition is  $|0\rangle \longleftrightarrow |1\rangle_+$  for the first row,  $|0\rangle \longleftrightarrow |1\rangle_0$  for the second row and  $|0\rangle \longleftrightarrow |1\rangle_-$  for the third row.

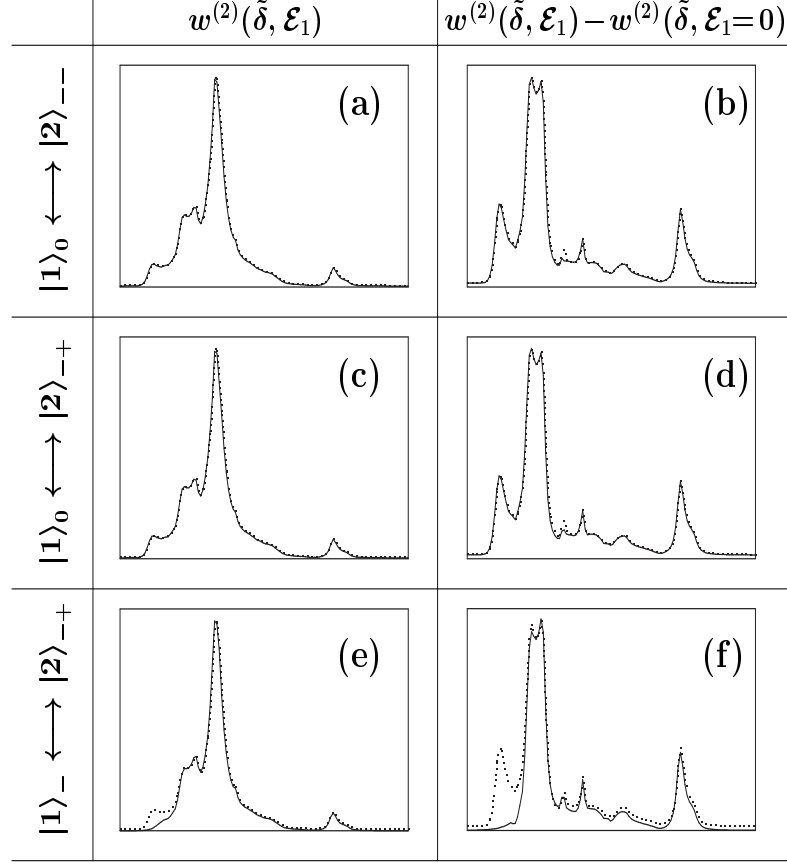


Figure 8: The 2PCR without (first column) and with (second column) background subtraction as the dotted line. The solid line corresponds to the 2PCR for an  $\omega_1$ -driven transition artificially suppressed in the numerical simulation. The suppressed transition is  $|1\rangle_0 \longleftrightarrow |2\rangle_{--}$  for the first row,  $|1\rangle_0 \longleftrightarrow |2\rangle_{-+}$  for the second row and  $|1\rangle_- \longleftrightarrow |2\rangle_{-+}$  for the third row.

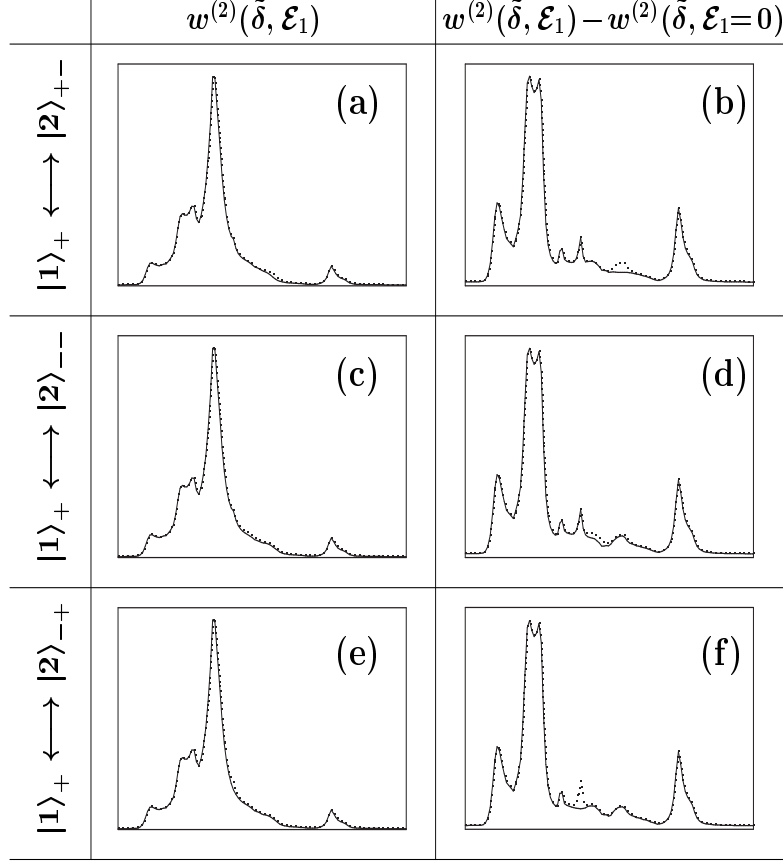


Figure 9: The 2PCR without (first column) and with (second column) background subtraction as the dotted line. The solid line corresponds to the 2PCR for an  $\omega_1$ -driven a transition artificially suppressed in the numerical simulation. The suppressed transition is  $|1\rangle_+ \longleftrightarrow |2\rangle_{+-}$  for the first row,  $|1\rangle_+ \longleftrightarrow |2\rangle_{--}$  for the second row and  $|1\rangle_+ \longleftrightarrow |2\rangle_{-+}$  for the third row.

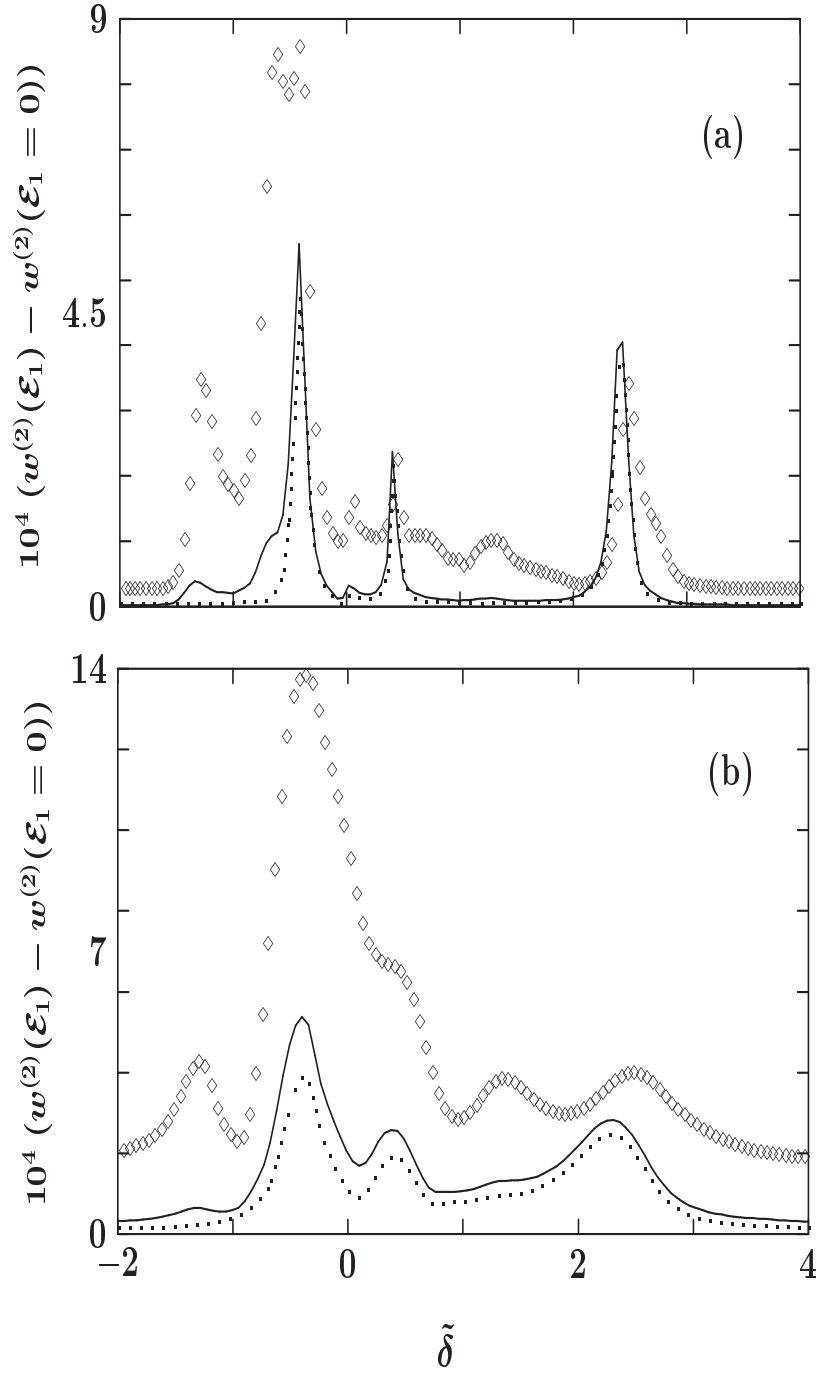


Figure 10: Two-photon count rate vs normalised scanning frequency for one atom (dotted line), two atoms ( $\diamond$ ) and a sparse atomic beam (solid line) with  $p_1/p_2 = 9$  for  $\mathcal{E}_1/\kappa = 1/\sqrt{2}$ ,  $\mathcal{E}_2/\kappa = \sqrt{2}$  and  $\gamma/\kappa = 2$  with (a)  $g_f = 63\kappa$  and (b)  $g_f = 9\kappa$ .